

**Contrasting physical controls on subsurface phosphorus transport to  
shallow groundwater ~~at different~~ at the hillslope ~~locations~~ seale**

M~~ae~~lle Fresne<sup>1,2,3</sup>, Phil Jordan<sup>2</sup>, Per-Erik Mellander<sup>1,3</sup>, Karen Daly<sup>3</sup>, Owen Fenton<sup>3</sup>

<sup>1</sup>Agricultural Catchments Programme, Teagasc, Johnstown Castle Environment Research  
Centre, Wexford, Co. Wexford, Ireland

<sup>2</sup>School of Geography and Environmental Sciences, Ulster University, Coleraine, UK

<sup>3</sup>Crops, Environment and Land Use Programme, Teagasc, Johnstown Castle Environment  
Research Centre, Wexford, Co. Wexford, Ireland

*Correspondence to:* M. Fresne (~~m~~Mae~~lle~~.fresne@hotmail.fr)

## Abstract

In well-drained agricultural catchments water flow through the unsaturated zone (USZ) to shallow groundwater (GW), and subsequent limiting soil phosphorus (P) attenuation, transport of phosphorus (P) to groundwater (GW) can be controlled by static and dynamic factors and ~~and where surface water is GW fed this can contribute lead~~ to elevated stream P concentrations ~~at the catchment outlet.~~ In order to better control P transport to GW at different hillslope locations, along hillslopes a spatial and temporal conceptual view of P transport through the USZ loss to GW must be developed. Initially ~~in the present study,~~ hillslope GW quality and rainfall data were examined for 2017 utilising a transect of piezometers at ~~upslope (US),~~ midslope (MS) and downslope (DS) locations. Two dominant scenarios emerged where GW P concentrations at DS were variable and MS remained low or at other times DS remained elevated and MS remained low. Two dominant scenarios emerged where GW P concentrations at DS and MS were simultaneously low or at other times DS became elevated and MS remained low. To examine ~~the~~ the potential physical reasons for such scenarios, potential reasons for such scenarios, a one-dimensional dual-porosity water flow hydrological transport model was developed for the USZunsaturated zone at DS and MS using rainfall and depth-specific soil ~~physical and~~ hydraulic data determined from soil water retention curve modelling from undisturbed soil cores. Results indicated that the DS zone was 29 % less compacted, had a higher total porosity of 28 % (macroporosity of 13 %), a higher saturated water content of 25 % but a lower soil saturated hydraulic conductivity ( $K_s$ ) of 62 % than the MS zone. This led to lower modelled cumulative water flow (74-78 % of total rainfall) compared to MS (76-80 %) and facilitated transport (higher sand content, soil saturated hydraulic conductivity ( $K_s$ ) and lower soil compaction) with higher flow peaks during higher total rainfall events (4.1-5.2 mm h<sup>-1</sup> at DS, 3.5-4.9 mm h<sup>-1</sup> at MS). This suggested that water flow in the USZ is facilitated and P attenuation processes are more

37 limited at DS during larger rainfall events contributing to higher GW P concentrations at DS,  
38 and is exacerbated with shallower GW mobilising soil P. ~~Higher modelled concentration~~  
39 ~~peaks towards higher GW P concentrations whereas the MS zone had more potential to~~  
40 ~~attenuate transport (lower soil  $K_s$  and higher soil compaction).~~ Hence, mitigation strategies  
41 should particularly focus on reducing P sources in the DS zone but this also indicates a need  
42 to identify “hotspots” of facilitated water flow and P transport to shallow GW using finer  
43 scale soil properties surveys.  
44 ~~Moreover, inter-annual variations of GW P concentrations at DS were related to rainfall and~~  
45 ~~GW level. Hence, mitigation strategies should particularly (but not exclusively) focus on~~  
46 ~~reducing P sources in the DS zone. This also indicates a need to identify “hotspots” of~~  
47 ~~facilitated transport to shallow GW using finer scale soil properties surveys. Here, this is~~  
48 ~~defined by low soil compaction, high sand content and soil  $K_s$ . However, challenges arise as~~  
49 ~~soil properties can vary in time with soil management and with the difficulty of assessing the~~  
50 ~~transport potential of deeper soil.~~

## 1. Introduction

Phosphorus (P) is a key nutrient for plant growth and food security (Cordell and White, 2014) but it can also be lost from agricultural land thereby contributing to the eutrophication of surface waters (Withers et al., 2014) which is a continuing global problem (Sinha et al., 2017). Within agricultural catchments, static (e.g. soil, subsoil and geology (Fenton et al., 2017)) and dynamic (e.g. climate (Mellander et al., 2018)) controls on P in groundwater (GW) and surface water are complex. Such controlling factors determine the timing, load, concentration and form of P delivered to a water body (Lintern et al., 2018). Concentrations of P in GW can be influenced by soil properties such as pH and clay % (Mabilde et al., 2017) as well as the presence of macropores or preferential flow paths (Bol et al., 2016; Julich et al., 2017; Fuchs et al., 2009). Bedrock P (sediments) and dissolution of P-rich minerals (McGinley et al., 2016) are also known as internal sources of P in GW. Temporal variations have been related to GW depth (Mabilde et al., 2017) influencing soil redox conditions and P release from Fe-oxides (Neidhardt et al., 2018; Dupas et al., 2015). Hydrological dynamics of hillslopes shallow subsurface flows are highly variable in space and time (Bachmair et al., 2012b) and controlling factors include rainfall (Lehmann et al., 2007; Duan et al., 2017), bedrock topography and permeability (Tromp-van Meerveld and Weiler, 2008; Graham et al., 2010) as well as soil properties (Bachmair and Weiler, 2012a): topography (Bachmair and Weiler, 2012a), infiltration capacity, hydraulic conductivity, drainable porosity, moisture content and vertical and lateral preferential flowpaths (Guo et al., 2019; Anderson et al., 2009; Wilson et al., 1990, 2017).

To complement field studies on P transport, numerous models are available and conveniently cover a wide range of spatial (from soil profile (e.g., HGS, HYDRUS, PHREEQC) to catchment scale (e.g., SWAT)) and temporal scales (from days (e.g., ADAPT) to years)

(Pferdmanges et al., 2020). Water flow models first needs to be developed and validated to model P transport through the unsaturated zone (USZ). HYDRUS 1D is of particular interest for water transport to GW as it is one of the few models explicitly set up for simulations on short periods such as single rainfall events and focuses on vertical flux. Moreover, it offers a wide range of options to simulate preferential (macropores) flow (dual-porosity, dual-permeability models), important for P transport, and can be adapted to P using complex and numerous specific parameters values and transformation rates (Radcliffe et al., 2015). This model has been used to investigate the vertical distribution and transport processes of P (Elmi et al., 2012) or predict P leaching (Agah et al., 2016), for example.

Despite GW P being subject to microbial cycling, subsurface transport, and immobilization (Neidhardt et al., 2018), processes possibly attenuating belowground P, GW contribution to stream P is a concern (Mellander et al., 2016). This can be indicated by a higher contribution of bioavailable P (to total P) associated with a greater proportion of baseflow in rivers (Schilling et al., 2017). Therefore, any interpretation of contrasting P concentrations in GW at different monitoring points within a hillslope must include a variety of these factors. Increased characterisation and knowledge of contrasting scenarios is vital if best management practices on hillslopes are to be implemented correctly (i.e. right measure, right place) to safeguard water quality (Sharpley, 2016). Catchment scale studies with river and GW data, combined with physical data (meteorological and soil data, GW level), have the best opportunity to reveal transport processes from soils to GW and also subsequent delivery to surface water (Melland et al., 2012; Mellander et al., 2016; Mellander et al., 2014).

Combined field and laboratory techniques have used undisturbed (Bacher et al., 2019) or disturbed (Pang et al., 2016) soil, subsoil and bedrock samples that develop datasets to run

model scenarios that best explain the transport of P to GW (Schoumans and Groenendijk, 2000; Schoumans et al., 2009). Different levels of data complexity (from simple to complex) affect transport model outcomes and it is therefore preferable where possible to collect undisturbed soil cores and develop soil physical and hydraulic parameters (Bünemann et al., 2018). Soil physical data such as porosity, saturated hydraulic conductivity ( $K_s$ ) or bulk density ( $\rho_b$ ), in combination with soil texture and water storage, can be used in models to assess water and solute transport dynamics through the ~~unsaturated zone~~USZ to GW (Fenton et al., 2015; Vero et al., 2014), in combination with site specific meteorological data (Gladnyeva and Saifadeen, 2013; Vero et al., 2014) and boundary conditions (Jacques et al., 2008; Vereecken et al., 2010). Combining high quality soil data with high resolution surface water, GW and meteorological data is an important approach towards a greater understanding of the major controls on P transport to shallow GW and thus provide important knowledge for GW P risk assessments. However, underground storage and release of P to GW and subsequent transit of P to surface water remains poorly understood (Gao et al., 2010).

The aim of this study was to address this knowledge gap and was undertaken in a meso-scale catchment observatory in Ireland with stream P dominantly delivered through below-ground pathways~~pressures assumed to be from GW P pathways~~. Mellander et al. (2016) had previously showed that long-term dissolved reactive P (DRP) concentrations at the stream outlet were consistently above the Environmental Quality Standard (EQS) of 0.035 mg P L<sup>-1</sup>. Initial testing of a multi-level borehole network in a connected hillslope revealed spatial and temporal fluctuations in P concentrations. Therefore, the present study examined the connected hillslope in greater detail with ~~three~~ objectives to:

1) ~~investigate~~determine the effect of soil hydraulic properties ~~on~~controlling water flow  
and subsequent P transport through the USZ at different hillslope  
locations~~hydrological P transport to GW along the hillslope~~;  
4) ~~investigate the effect of dynamic physical controls (rainfall, GWL) on temporal~~  
~~variations in water flow and shallow GW P concentrations.~~

2)  
~~examine variations in GW P concentrations in relation to dynamic physical controls;~~  
~~reveal contrasting physical controls on P transport to GW at the hillslope scale.~~

## 2. Materials and methods

### 2.1. Site description

The meso-scale agricultural catchment (7.58 km<sup>2</sup>) (Fealy et al., 2010) is located in the south-west of Ireland (Co. Cork). A summary of catchment characteristics and long-term outlet concentrations of total dissolved P (TDP), DRP, dissolved unreactive P (DUP = TDP – DRP), iron (Fe) and dissolved organic carbon (DOC) are presented in **Table 1**. The catchment is dominated by ~~well-drained~~well-drained soils (based on diagnostic features of the soil profile to 1 m and a soil survey at 1:25 000) and permeable bedrock, which results in high levels of infiltration and a ~~groundwater-GW~~-fed main river (Dupas et al., 2017a; Mellander et al., 2016).

Table 1: Summary of dominant catchment characteristics.

<b>Average annual rainfall<sup>a</sup></b>	1 <del>10625</del> mm
<b>Average effective rainfall<sup>a</sup></b>	<del>582600</del> mm
<b>Soil type<sup>b</sup></b>	Typical Brown Earth <u>(Cambisol)</u> and Typical Brown Podzols <u>(Podzol)</u> (84 %)

<b>Dominant Soil Drainage class<sup>c</sup></b>	<del>Well-drained</del> <u>Well-drained</u>
<b>Geology<sup>d</sup></b>	Highly permeable sandstone, mudstone and siltstone
<b>Land use</b>	Grassland (84 %), Arable (6 %)
<b>Outlet water chemistry<sup>eb</sup></b>	0.119 mg TDP L <sup>-1</sup> , 0.078 mg DRP L <sup>-1</sup> , 0.029 mg DUP L <sup>-1</sup> , 0.41 mg Fe L <sup>-1</sup> , 1.08 mg DOC L <sup>-1</sup>

<sup>a</sup>Meteorological station located within the catchment see Figure 1, 2010-2016

<sup>b</sup>Irish classification system (World Reference Base classification system)

<sup>c</sup>Irish classification system (well-drained soil: no obvious sign of impeded drainage (mottling) throughout the solum. Exception where under pasture, sparse mottling may occur in topsoil)

<sup>d</sup>Geological Survey Ireland

<sup>eb</sup>Monthly grab samples taken within the catchment see Figure 1, 2010-2016 (DOC 2012-2016)

The hillslope study site consists of a transect of ~~multi-level~~ piezometers ~~screened in shallow bedrock and~~ installed to monitor GW level, ~~gradients~~ and water quality (~~Fig. 1~~). ~~For the purpose of the present study only the shallow piezometers were used~~ at the downslope (DS) ~~and~~, midslope (MS) ~~and upslope (US)~~ locations (**Fig. 1, Fig. 2**). Piezometer screen depths were 4-7 m at DS ~~and~~, 10.5-13.5 m at MS ~~and 13-16 m at US~~. Monthly grab samples were taken within the screen depth for chemical analysis using a 200 ml double valve bailer (Solinst, Canada). Samples were filtered (0.45 µm Sartorius) and TDP and DRP were analysed by spectrophotometry after alkaline persulphate oxidation (for TDP) (Askew, 2005) and after ascorbic acid reduction (for TDP and DRP) (method detection limit (MDL): 0.005 mg L<sup>-1</sup>) (Askew and Smith, 2005), ~~respectively~~. Dissolved unreactive P (DUP) was noted as the difference between TDP and DRP. ~~Iron and manganese (Mn) were analysed on a Varian Vista-MPX-CCD Simultaneous ICP-OES, DOC was analysed by a non-Diffractive Infra-Red~~



(~~NDIR~~) detector after acidification and combustion and nitrate ( $\text{N-NO}_3^-$ ) was calculated as the difference between total oxidized nitrogen (TON) and nitrite ( $\text{N-NO}_2^-$ ) analysed on an Aquakem 600A (Thermo Scientific, Finland) after hydrazine reduction (MDL:  $0.1 \text{ mg L}^{-1}$ ) and phosphoric acid diazotization (MDL:  $0.006 \text{ mg L}^{-1}$ ), respectively (Kamphake et al., 1967). At time of sampling in the field the oxidation reduction potential (ORP) of GW was measured using an Aquaread AP 700 multiparameter probe. Water level and gradients between multi-level piezometers was recorded at high resolution using a Solinst water level logger to ascertain ~~direction of recharge~~ infiltration versus up welling. Average (2010-2016) depths to GW level (DGWL) were  $0.30 \pm 0.01 \text{ m}$  at DS and,  $7.20 \pm 0.28 \text{ m}$  at MS ~~and~~  $11.9 \pm 0.23 \text{ m}$  at US.

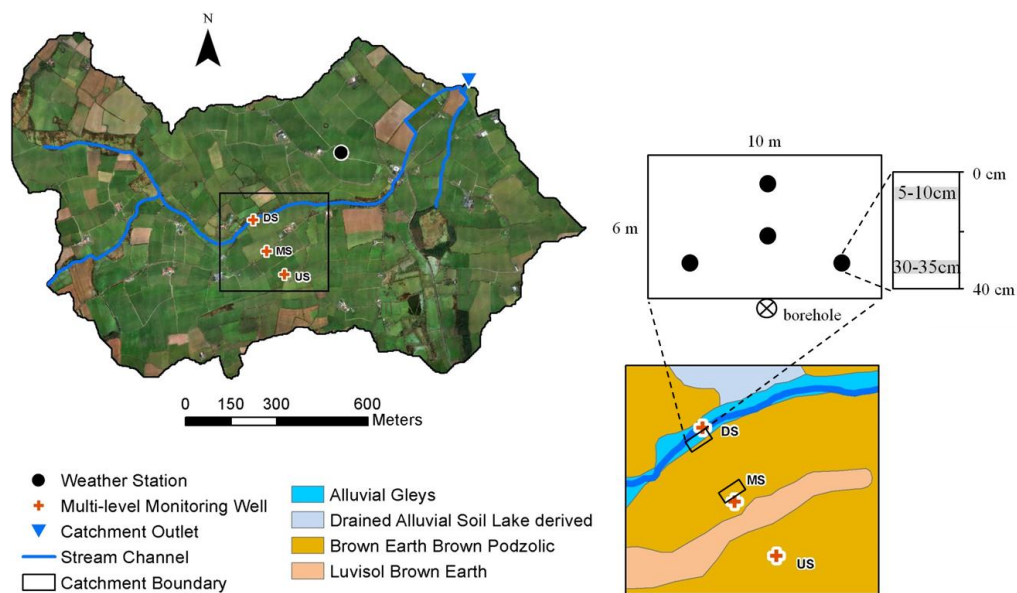


Figure 1 (~~in color~~): Location of the hillslope piezometers (DS, MS and US) within the context of the catchment, stream channel and outlet. The schematic on the lower right indicates soil types and intact coring location and depth of sampling around DS and MS.

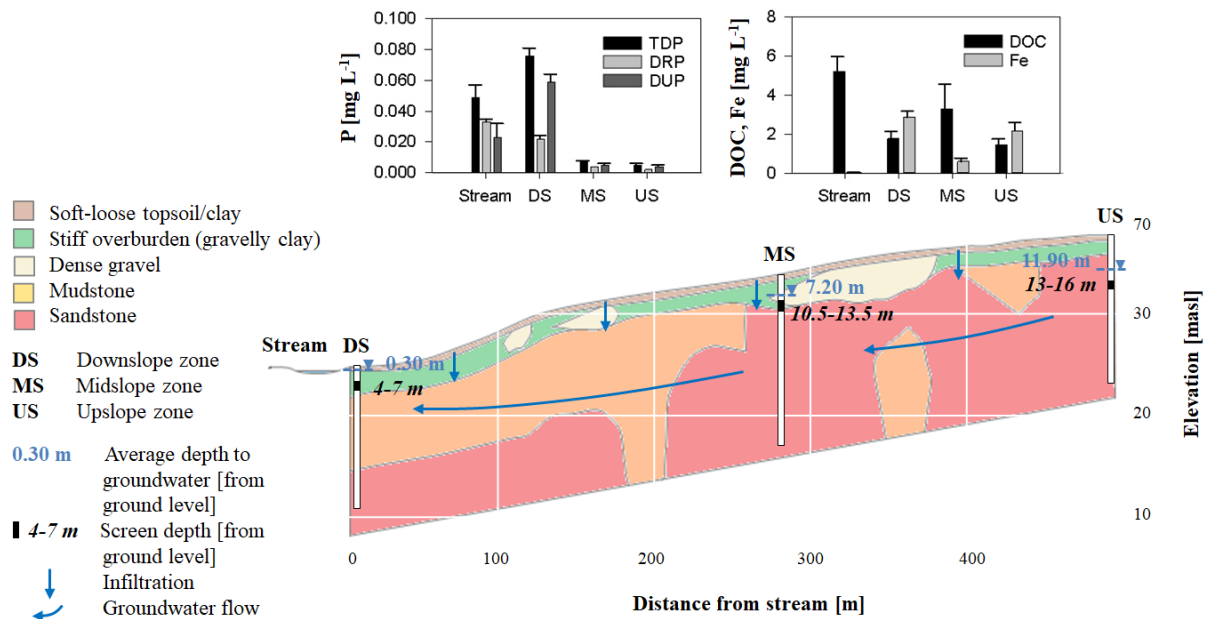


Figure 2: ~~(in color)~~ Geological cross section of the study hillslope showing the location of the piezometers (McAleer et al., 2017; Mellander et al., 2014). Also illustrated are the stream and the groundwater chemistry at the study sites (based on monthly grab samples, 2010-2016 - DOC 2013-2016).

Using long terms datasets average concentrations of dissolved P and related parameters are shown in **Figure 2**. Site DS had higher P concentrations than at MS and in terms of DRP the stream data indicated long-term (2010-2016) average concentrations above or close to the EQS. It should be noted that there are soil type (based on 1 m depth only) differences at DS and MS/US with ~~Humic~~-Alluvial Gley ~~/Gleyic Brown Alluvial soil (Gleysol)~~ and Typical Brown Earth/Podzols ~~(Cambisol/Podzol)~~, respectively.

## 2.2. Field methods - meteorological and soil data

For the purposes of the present study meteorological data taken from a Campbell Scientific BWS-200 weather station (**Fig. 1**) from January 2017 to December 2017 were examined. Absence of rainfall for at least 12 hours was used to separate one rainfall event from another

(Ibrahim et al., 2013; Kurz et al., 2005) and only events having at least 5 mm rainfall were included in this process. These data were further sub-divided into 5 rainfall event types (A-E) depending on the total rainfall amount (A = 5.0-9.9 mm, B = 10.0-19.9 mm, C = 20.0-29.9 mm, D = 30.0-39.9 mm, E =  $\geq 40$  mm). Using the hybrid soil moisture deficit (SMD) model of Schulte et al. (2005) infiltration [mm] was estimated. ~~Both rainfall~~ Rainfall, infiltration and SMD data were used ~~during the interpretation of GW TDP concentrations data and~~ to develop modelling scenarios to investigate explain differences in hydrological transport dynamics P concentrations over time in the USZ at DS and MS locations.

Undisturbed soil cores (8 cm diameter, 5 cm height) were extracted at two depths (5 to 10 cm, 30 to 35 cm, 4 replicates) within a sampling grid close to DS and MS (**Fig. 1**). One additional soil core was taken at each site and depth. Using this strategy, ~~2016~~ soil cores were collected between January and March 2018 before organic fertiliser (i.e. cattle slurry) was applied.

## **2.3. Laboratory methods**

### **2.3.1. Undisturbed soil physical and hydraulic data**

Soil  $\rho_b$  [g cm<sup>-3</sup>] was initially measured using the destructed additional soil cores and subsequently using the destructed undisturbed soil cores following soil physics hydraulic analysis. This was preferred to the direct determination via soil water retention curve (SWRC) analysis as results were distorted by the presence of stones in the undisturbed soil cores. Samples were oven-dried at 105 °C for 48 h and then weighed. Stones above 2 mm were extracted, weighed and their volume was determined. Soil  $\rho_b$  was calculated by dividing the soil dry weight by the soil volume. Soil particle size distribution (PSD – sand, silt and clay content [%] (Brady and Weil, 2008)), using the pipette method (Avery and Bascomb, 1974), and soil texture wereas -later determined using the 2 mm sieved soil from the additional soil

~~cores, using disturbed soil samples taken at both locations and depths which were used to ascertain particle size distribution (PSD, sand, silt and clay content [%] (Brady and Weil, 2008)) using the pipette method (Avery and Bascomb, 1974). Soil  $\rho_b$  [ $\text{g cm}^{-3}$ ] was measured using the disturbed soil samples and subsequently using the destructured undisturbed soil cores following soil physics hydraulic analysis. This was preferred to the direct determination via soil water retention curve (SWRC) analysis as results were distorted by the presence of stones in the undisturbed soil cores. Samples were oven-dried at 105 °C for 48 h and then weighed. Stones were extracted, weighed and their volume was determined. The  $\rho_b$  was calculated by dividing the soil dry weight by the soil volume.~~

The undisturbed cores were transferred to the laboratory for the continuous hydraulic measurement of a SWRC in terms of volumetric water content  $\theta_v$  using an evaporation method. The Hyprop apparatus (UMS GmbH, Munich, Germany) (Bezerra-Coelho et al., 2018) was used for this purpose and a detailed procedure ~~has been~~ is described in Bacher et al. (2019). In summary, the raw Hyprop data from the direct SWRC approach were ~~then~~ fitted to the bimodal van Genuchten model of Durner (Durner, 1994) - for the retention fitting - with the Mualem-constraint (Mualem, 1976) - for the  $K_s$  fitting - which predicts the shape of the conductivity function from the shape of the retention function, to obtain the hydraulic parameters needed for the subsequent flow modelling~~modelling phase~~. This dual-porosity model is a weighted superposition of two van Genuchten functions and is more suitable than the unimodal models to describe the retention functions of structured soils with bimodal pore-size characteristics. It also fitted better to the data than the unimodal constrained model of van Genuchten (1980). The detailed SWRC modelling steps and procedures are described in **S1** in the Supplement.

Hydraulic retention and conductivity parameters were then generated for each soil core: soil residual  $\theta_r$  and saturated  $\theta_s$  water contents [ $\text{cm}^3 \text{ cm}^{-3}$ ], soil  $K_s$  [ $\text{cm d}^{-1}$ ], SWRC shape parameters  $n_1$  and  $n_2$  [~~undimensional~~undimensional; -],  $\alpha_1$  and  $\alpha_2$  [ $\text{cm}^{-1}$ ] and  $\omega_2$  [-]. A statistical analysis ( $E_{\text{RMS}}$ ) quantified the quality of the fits for both retention and conductivity.

To further interpret varied conditions at DS and MS additional parameters that could control transport to GW were calculated including total porosity  $\phi$  [%], air capacity  $\varepsilon$  [%], macro-, meso- and microporosity [%]. Detailed calculation steps are presented in S2. A list of abbreviations of soil physical and hydraulic parameters is presented in Table 2.

Table 24: List of abbreviations of soil physical and hydraulic parameters

<u>Symbol</u>	<u>Abbreviation</u>
<u><math>\rho_b</math></u>	<u>Bulk density</u>
<u><math>\theta_r</math></u>	<u>Residual water content</u>
<u><math>\theta_s</math></u>	<u>Saturated water content</u>
<u><math>a</math></u>	<u>SWRC shape parameter: controls the air-entry pressure</u>
<u><math>n</math></u>	<u>SWRC shape parameter: controls the bending of the retention curve around the air-entry region and the curvature towards the residual water content</u>
<u><math>K_s</math></u>	<u>Saturated hydraulic conductivity</u>
<u><math>l</math></u>	<u>Pore connectivity</u>
<u><math>\omega</math></u>	<u>Weight of each van Genuchten sub-function</u>
<u><math>\phi</math></u>	<u>Total porosity</u>
<u><math>\varepsilon</math></u>	<u>Air capacity</u>

### 2.3.2. Modelling scenarios of ~~phosphorus—water flow~~hydrological—transport to groundwater

Simulations were conducted using Hydrus 1D (Šimůnek et al., 2008; Šimůnek et al., 2013), coupled with appropriate meteorological and soil physical data, boundary conditions, and

resulting water flow breakthrough curve at the bottom of the soil profiles ~~was~~<sup>ere</sup> used to assess ~~P~~water hydrological transport dynamics to GW through the USZ at DS and MS (**Fig. 3**).

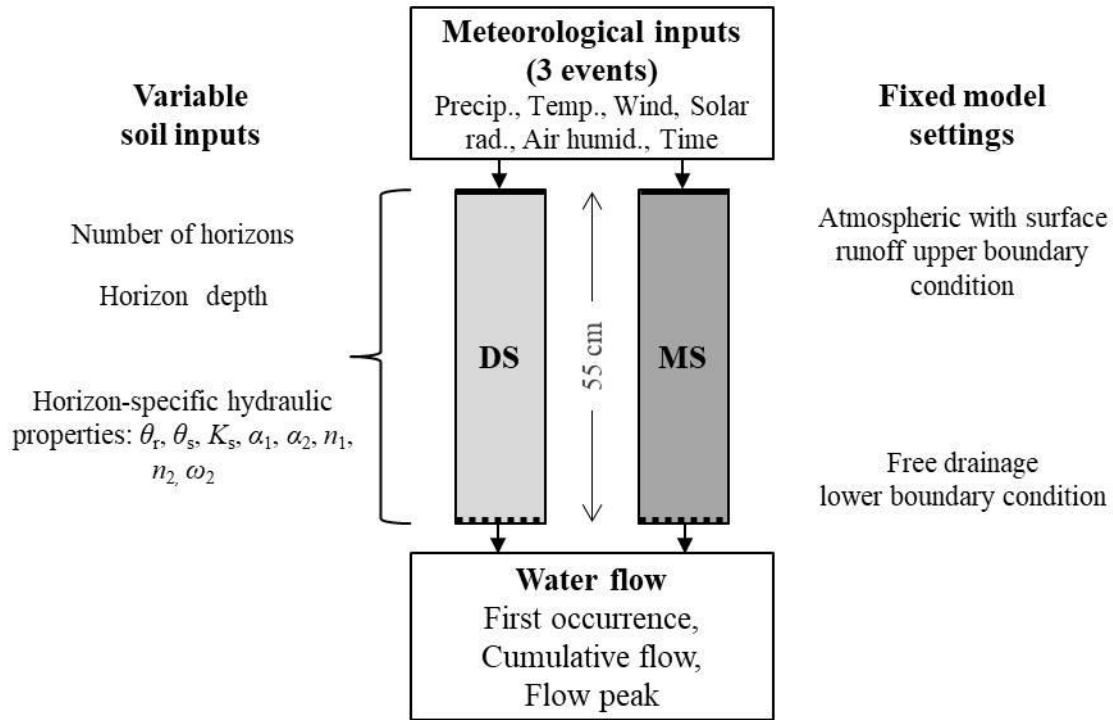


Figure 3: Conceptual diagram indicating input parameters, boundary conditions, soil horizon characteristics and model outputs.

Examination of soil profiles at both sites resulted in the delineation of soil horizons and the determination of the soil profiles depths (55 cm for both sites). To build a soil profile for the dual-porosity model the physical and hydraulic data taken from the undisturbed soil cores were used for both DS and MS locations. Specifically  $\theta_r$  and  $\theta_s$  [ $\text{cm}^3 \text{ cm}^{-3}$ ],  $K_s$  [ $\text{cm h}^{-1}$ ], SWRC shape parameters  $\alpha_1$  and  $\alpha_2$  [ $\text{cm}^{-1}$ ],  $n_1$  and  $n_2$  [-], and  $\omega_2$  [-] ~~and soil  $\rho_b$  [ $\text{g cm}^{-3}$ ]~~ were used as input parameters. Median values of soil physical and hydraulic parameters (Table 3) were used to choose the replicate which was the most representative of the site and depth. Choice was first based on the  $K_s$  value which was deemed to be the most critical for water transport, then on  $\theta_s$  when two replicates were similarly close to the median value. For each

~~depth the replicate which showed the best fit ( $E_{RMS}$ ) to the retention and conductivity models was chosen.~~ Hydraulic data of the selected soil core were applied to the soil horizon including this soil core sampling depth and, when no hydraulic data were available for a horizon, the data from the upper horizon were applied. Soil pore connectivity parameter  $l$  was set at 0.5 [-] following the original study by Mualem (1976). To determine initial soil moisture conditions along the soil profiles for the subsequent transient flow modelling, steady-state flow was first modelled. A constant water flux of  $0.0068 \text{ cm h}^{-1}$  (average annual infiltration (precipitation – potential evaporation) over the period 2010-2017 in the study catchment) with free drainage was applied on both soil profiles at DS and MS.

To investigate the effect of variable rainfall conditions on water flow through the USZ, transient flow was later modelled at the bottom of the soil profiles at ~~For each location~~ DS and MS with one model run ~~was~~ carried out for each contrasting (in terms of total rainfall and duration) rainfall event (R1, R2 and R3) leading to six model scenarios in total. The model was started at the beginning of the rainfall event and was ended the hour preceding the beginning of the following rainfall event.

Atmospheric upper boundary conditions with surface runoff were assigned to the model in order to examine the role of soil hydraulic properties and rainfall patterns on water transport. The contrasting rainfall events were expected to affect ~~differently~~ water transport dynamics differently (and subsequently chemical P attenuation processes). Hourly (Vero et al., 2014) total precipitation (cm), maximum and minimum temperatures [ $^{\circ}\text{C}$ ], average wind speed [ $\text{km d}^{-1}$ ], average solar radiation [ $\text{MJ cm}^{-2}$ ] and average air humidity [%] data from 2017 were used as input parameters. ~~Solute dispersivity was set at 10 % of soil profile depth (Fetter, 2008; Šimůnek et al., 2013). A conservative solute was used in order to examine the role of~~

~~soil hydraulic properties on the potential for P transport to GW. Thus, no soil chemical input data were used in the models and chemical P attenuation processes in soil are not considered here. Conservative solute initial concentration at the soil surface was set at  $10 \text{ mmol cm}^{-3}$  and 1 cm precipitation was applied with no evaporation, in order to initiate vertical solute movement into the soil profile.~~ Free drainage was specified as the lower boundary condition (Jacques et al., 2008).

## 2.4. Data and statistical analysis

For objective 1, ~~descriptive statistics of soil parameters were carried out for each depth and site. Soil  $K_s$  values with  $E_{RMS} > 0.90$  were removed for this purpose as they were deemed to be not representative of the soil core.~~ A analysis of variance (ANOVAs) was ~~later~~ used to investigate significant ( $P < 0.05$ ) differences of soil properties between depths within each site and between sites for each depth. Residuals plots were used to assess the normal distribution of the residuals and the equal variance of the data; data were log transformed before statistical analyses when those conditions were not met. Trends were studied when the variation between replicates was very high (e.g.  $K_s$ ). Pearson ~~R~~ correlations were used to measure the degree of relationship between soil parameters. Statistical analysis was carried out using R Studio 3.5.2.

## 3. Results

### 3.1. Soil hydraulic properties

Detailed soil physical and hydraulic data for all undisturbed soil cores replicates of sites DS and MS are shown in Tables ~~S~~-S3 and ~~Table~~ S4, respectively. ~~Descriptive statistics of soil physical and hydraulic parameters for each depth and site are shown in Table 32.~~ Below is a description of the overall (at the scale of the sampling area, including the four replicates)



variations observed between sites and depths. ~~The SWRC shape parameters  $\alpha_1$  and  $\alpha_2$ ,  $n_1$  and  $n_2$ ,  $\omega_2$ , as well as  $\theta_s$  and  $\theta_r$  are not presented as they are not considered to be the main parameters controlling hydrological transport to GW. A detailed description of hydraulic parameters is presented in S5.~~ Soil at DS is a Sandy Loam whereas MS soil has a Loamy texture.

Median soil  $\rho_b$  was higher (not significantly) at MS than DS for both shallow and deeper soil cores. Soil  $\rho_b$  increased with depth (not significantly) in each site: from 0.85 to 0.95 g cm<sup>-3</sup> at DS, and from 1.22 to 1.28 g cm<sup>-3</sup> at MS. Soil organic matter content (OM %) was higher at DS (8.3 %) than at MS (4.6 %).

Median soil  $\theta_r$  was equal to 0 cm<sup>3</sup> cm<sup>-3</sup> for shallow soil at DS and at MS while it was equal to 0.06 cm<sup>3</sup> cm<sup>-3</sup> in deeper soil at DS. Median soil  $\theta_s$  was higher (not significantly) at DS than MS for both shallow and deeper soil cores. Soil  $\theta_s$  decreased with depth (not significantly) in each site: from 0.64 to 0.59 cm<sup>3</sup> cm<sup>-3</sup> at DS, and from 0.54 to 0.47 cm<sup>3</sup> cm<sup>-3</sup> at MS.

At both sites and for both depths, soil  $K_s$  was variable. Median  $K_s$  was higher (not significantly) at DS than MS for shallow soil cores and higher at MS than DS for deeper soil cores. Soil  $K_s$  decreased with depth (not significantly) at each site: from 1-914 to 209 cm d<sup>-1</sup> at DS, and from 1-866 to 1-468 cm d<sup>-1</sup> at MS.

Median  $\phi$  was higher (not significantly) at DS than MS for both shallow and deeper soil cores. Soil  $\phi$  decreased with depth (not significantly) at each site: from 68 to 64 % at DS, and from 54 to 51 % at MS. Median  $\varepsilon$  was higher (not significantly) at DS than MS for both shallow and deeper soil cores. Soil  $\varepsilon$  increased with depth (not significantly) at each site: from 21 to 26 % at DS, and from 14 to 19 % at MS.

Median soil macroporosity was higher (not significantly) at DS than MS for both shallow and deeper soil cores. Soil macroporosity significantly decreased with depth at MS - from 43 to 39 % - but not significantly at DS - from 50 to 41 %. Median soil mesoporosity and microporosity were comparable between DS and MS for both shallow and deeper soil cores, and both decreased with depth.

Soil  $\rho_b$  was strongly and significantly correlated to sand ( $R = - 0.828$ ), silt ( $R = 0.792$ ) and clay % ( $R = 0.833$ ) as was soil  $\phi$  ( $R = 0.828$ ,  $R = - 0.794$ ,  $R = - 0.829$ , respectively). Soil air capacity  $\varepsilon$  was correlated to clay % ( $R = - 0.503$ ).

Table 32: Descriptive statistics of soil hydraulic parameters for DS and MS

Site	Depth		$\rho_b$	$\alpha_1$	$n_1$	$\alpha_2$	$n_2$	$\omega_2$	$\theta_r$	$\theta_s$	$K_s$	$\phi$	macro	meso	micro	$\varepsilon$
			$\text{g cm}^{-3}$	$\text{cm}^{-1}$	-	$\text{cm}^{-1}$	-	-	$\text{cm}^3 \text{cm}^{-3}$	$\text{cm}^3 \text{cm}^{-3}$	$\text{cm d}^{-1}$	%	%	%	%	%
DS	5-10 cm	AVERAGE	0.89	0.292	2.743	0.103	1.313	0.630	0.03	0.63	2197 <sup>a</sup>	66	49	6	2	22
		MEDIAN	0.85	0.334	1.643	0.010	1.259	0.638	0.00	0.64	1914 <sup>a</sup>	68	50	6	2	21
		MAX	1.05	0.500	6.267	0.391	1.486	0.822	0.13	0.69	4110 <sup>a</sup>	69	53	9	3	28
		MIN	0.80	0.002	1.418	0.002	1.248	0.423	0.00	0.55	567 <sup>a</sup>	60	43	5	1	18
		SD	0.10	0.216	2.040	0.166	0.100	0.142	0.06	0.05	1460 <sup>a</sup>	4	4	2	1	4
	30-35 cm	AVERAGE	0.95	0.365	1.460	0.149	1.353	0.687	0.10	0.58	829	64	40	4	1	24
		MEDIAN	0.95	0.392	1.336	0.047	1.342	0.674	0.06	0.59	209	64	41	4	1	26
		MAX	1.04	0.500	2.159	0.500	1.591	0.943	0.27	0.63	2892	67	50	6	3	36
		MIN	0.86	0.177	1.010	0.001	1.135	0.459	0.00	0.51	7	60	28	1	0	9
		SD	0.06	0.140	0.440	0.206	0.164	0.177	0.11	0.04	1201	2	8	2	1	10
MS	5-10 cm	AVERAGE	1.20	0.139	1.376	0.174	1.438	0.490	0.00	0.55	2981	54	45	6	2	14
		MEDIAN	1.22	0.118	1.376	0.097	1.408	0.503	0.00	0.54	1866	53	43	7	2	14
		MAX	1.31	0.320	1.522	0.500	1.738	0.630	0.00	0.67	7762	59	53	8	3	17
		MIN	1.07	0.001	1.231	0.001	1.198	0.326	0.00	0.47	431	50	40	4	1	9
		SD	0.10	0.140	0.115	0.203	0.237	0.109	0.00	0.08	2835	4	5	2	1	3
	30-35 cm	AVERAGE	1.27	0.250	1.239	0.012	1.545	0.525	0.07	0.48	2990 <sup>b</sup>	51	35	4	1	19
		MEDIAN	1.28	0.250	1.274	0.001	1.564	0.463	0.00	0.47	1468 <sup>b</sup>	51	39	4	1	19
		MAX	1.40	0.500	1.400	0.047	1.753	0.904	0.27	0.52	6464 <sup>b</sup>	57	43	6	2	22
		MIN	1.12	0.000	1.010	0.000	1.298	0.269	0.00	0.44	1038 <sup>b</sup>	46	18	0	0	15
		SD	0.10	0.181	0.145	0.020	0.168	0.236	0.12	0.03	2463 <sup>b</sup>	4	10	2	1	2

370 <sup>a</sup>Without replicate 3 for which  $E_{RMS} K_s = 0.9046$

371 <sup>b</sup>Without replicate 2 for which  $E_{RMS} K_s = 0.9291$

Average soil  $\rho_b$  was higher (not significantly) at MS than DS for both shallow and deeper soil cores. Soil  $\rho_b$  increased with depth (not significantly) in each site: from 0.85 to 0.95 g cm<sup>-3</sup> at DS, and from 1.22 to 1.28 g cm<sup>-3</sup> at MS. Soil organic matter content (OM %) was higher at DS (8.3 %) than at MS (4.6 %).

Median soil  $\theta_r$  was equal to 0 for shallow soil at DS and at MS while it was equal to 0.06 in deeper soil at DS. Median soil  $\theta_s$  was higher (not significantly) at MS than DS for both shallow and deeper soil cores. Soil  $\theta_s$  decreased with depth (not significantly) in each site: from 0.64 to 0.59 cm<sup>3</sup> cm<sup>-3</sup> at DS, and from 0.54 to 0.47 cm<sup>3</sup> cm<sup>-3</sup> at MS.

At both sites and for both depths, soil  $K_s$  were variable. Median  $K_s$  was higher (not significantly) at DS than MS for shallow soil cores and higher at MS than DS for deeper soil cores. Soil  $K_s$  decreased with depth (not significantly) at each site: from 1 914 to 209 cm d<sup>-1</sup> at DS, and from 1 866 to 1 468 cm d<sup>-1</sup> at MS.

Median  $\phi$  was higher (not significantly) at DS than MS for both shallow and deeper soil cores. Soil  $\phi$  decreased with depth (not significantly) at each site: from 68 to 64 % at DS, and from 54 to 51 % at MS. Median  $c$  was higher (not significantly) at DS than MS for both shallow and deeper soil cores. Soil  $c$  increased with depth (not significantly) at each site: from 21 to 26 % at DS, and from 14 to 19 % at MS.

Median soil macroporosity was higher (not significantly) at DS than MS for both shallow and deeper soil cores. Soil macroporosity significantly decreased with depth at MS; from 43 to 39 % but not significantly at DS; from 50 to 41 %. Median soil mesoporosity and microporosity were comparable between DS and MS for both shallow and deeper soil cores, and both decreased with depth.

~~Soil  $\rho_b$  was strongly and significantly correlated to sand ( $r = -0.828$ ), silt ( $r = 0.792$ ) and clay % ( $r = 0.833$ ) as was soil  $\phi$  ( $r = 0.828$ ,  $r = -0.794$ ,  $r = -0.829$ , respectively). Air capacity was correlated to clay % ( $r = -0.503$ ).~~

Soil physical and hydraulic data used as input parameters in Hydrus 1D are presented in **Table 42**. ~~Spatial variations (between depths and sites) in soil parameters used as input variables, only the replicate showing the best fit ( $E_{RMS}$ ) to the retention and conductivity models was chosen. Values~~ were in accordance with the overall tendencies observed ~~between/within depths and sites and~~ described ~~explained~~ previously. ~~An exception exists for the  $K_s$  values due to the variability between replicates.~~

410 | Table ~~42~~: Summary of soil ~~physical and~~ hydraulic data used as input parameters in Hydrus  
411 | 1D.

Site	Horizon depth	$\theta_r$	$\theta_s$	$\alpha_1$	$n_1$	$K_s$	$l$	$\omega_2$	$\alpha_2$	$n_2$
		$\text{cm}^3$ $\text{cm}^{-3}$	$\text{cm}^3$ $\text{cm}^{-3}$	$\text{cm}^{-1}$	-	$\text{cm h}^{-1}$	-	-	$\text{cm}^{-1}$	-
DS	0-23 cm	0.00	0.63	0.500	1.816	80	0.5	0.618	0.004	1.256
	23-43 cm	<del>0.000</del>	<del>0.600</del>	<del>0.2840</del>	<del>1.174</del>	<del>17420</del>	<del>0.5</del>	<del>0.610</del>	<del>0.0010</del>	<del>1.591</del>
		<del>.00</del>	<del>.51</del>	<del>177</del>	<del>2.159</del>		<del>0.5</del>	<del>0.737</del>	<del>0.00</del>	<del>1.135</del>
	43-55 cm	<del>0.000</del>	<del>0.600</del>	<del>0.2840</del>	<del>1.174</del>	<del>17420</del>	<del>0.5</del>	<del>0.610</del>	<del>0.0010</del>	<del>1.591</del>
		<del>.00</del>	<del>.51</del>	<del>177</del>	<del>2.159</del>		<del>0.5</del>	<del>0.737</del>	<del>0.00</del>	<del>1.135</del>
MS	0-25 cm	<del>0.000</del>	<del>0.570</del>	<del>0.3200</del>	<del>1.522</del>		<del>0.5</del>	<del>0.630</del>	<del>0.0040</del>	<del>1.214</del>
		<del>.00</del>	<del>.51</del>	<del>0.01</del>	<del>1.449</del>	<del>9418</del>	<del>0.5</del>	<del>0.483</del>	<del>1.91</del>	<del>1.198</del>
	25-55 cm	<del>0.000</del>	<del>0.480</del>	<del>0.5000</del>	<del>1.400</del>		<del>0.5</del>	<del>0.516</del>	<del>0.0010</del>	<del>1.298</del>
		<del>.00</del>	<del>.44</del>	<del>306</del>	<del>1.311</del>	<del>6143</del>	<del>0.5</del>	<del>0.410</del>	<del>0.01</del>	<del>1.629</del>

412 |

413 | **3.2. Rainfall events, soil moisture deficit, water table depth and groundwater quality**

414 | Rainfall during 2017 is presented in **Figure 4a**. During ~~this~~ ~~that~~ year 56 rainfall events were  
415 | categorised as follows: 18 events A, 21 events B, 6 events C, 9 events D and 2 events E  
416 | (Table ~~S56~~, A = 5.0-9.9 mm, B = 10.0-19.9 mm, C = 20.0-29.9 mm, D = 30.0-39.9 mm, E =  
417 |  $\geq 40$  mm).

418 |

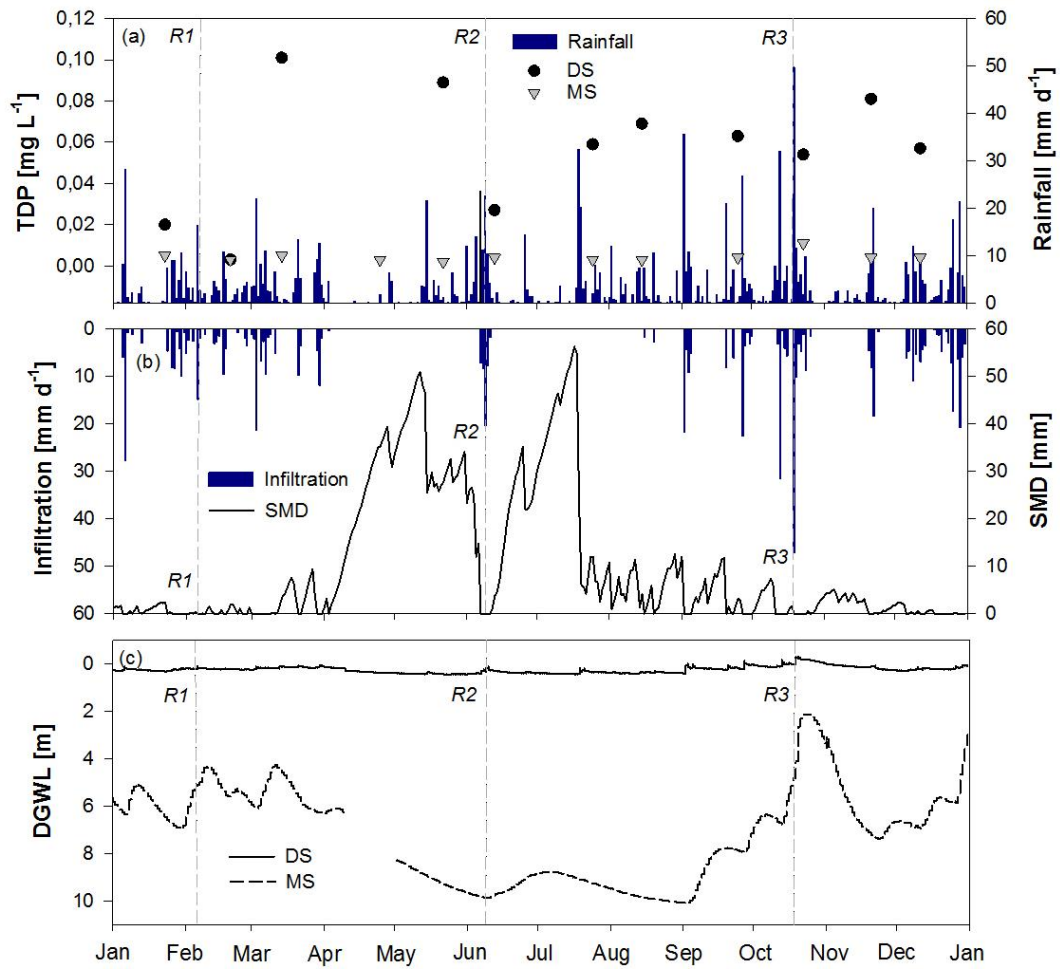


Figure 4: Evolution of (a) monthly groundwater TDP concentrations at sites DS (circle) and MS (square) and daily rainfall, (b) daily infiltration and soil moisture deficit and (c) depth to GWL over the study year 2017. Locations of the three study rainfall events (R1, R2 and R3) are also shown.

Rainfall event R1 [B; long duration with low total rainfall] occurred from the 6<sup>th</sup> to 7<sup>th</sup> of February, R2 [D; short duration with high total rainfall] from the 9<sup>th</sup> to 10<sup>th</sup> of June and R3 [E; long duration with high total rainfall] from the 18<sup>th</sup> to 19<sup>th</sup> of October. Event and pre-event characteristics are shown in **Figure 5**. Total rainfall was the highest for R3 and the smallest for R1 (50.6 and 19 mm, respectively), while maximum rainfall intensity was the smallest for R1 (3.2 mm h<sup>-1</sup>) and comparable between R2 and R3 (6.2 and 6.4 mm h<sup>-1</sup>, respectively).

Rainfall event R3 was the longest (40 h) while R2 was the shortest (15 h). Infiltration during the event was the highest for R3 and the lowest for R1 (47.1 and 16.8 mm, respectively). Pre-event total rainfall (previous 7 days) was the lowest for R1 (25.4 mm) and was comparable between R2 and R3 (55.8 and 57.2 mm, respectively).

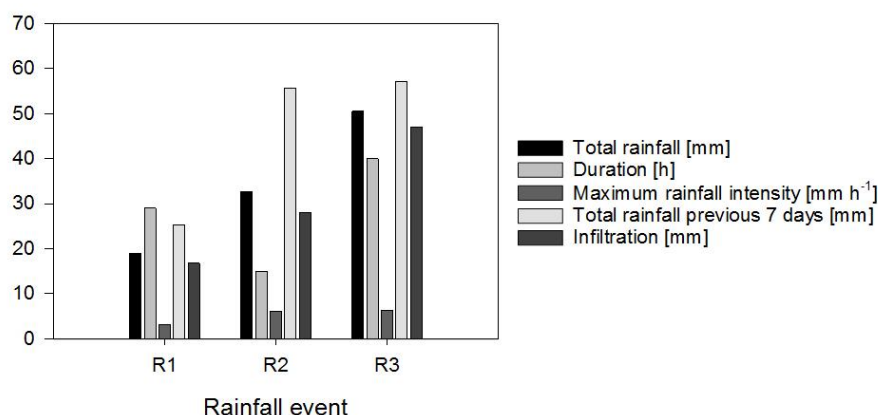


Figure 5: Summary of events and pre-events characteristics.

Daily SMD and infiltration for sites DS and MS (~~well-drained~~well-drained) over the year 2017 are shown in **Figure 4b**. Frequent rainfall from January to March and from September to December led to SMD less than 10 mm and frequent infiltration with an infiltration -peak of 47 mm occurring in mid-October. From April to July, less rainfall led to increasing SMD with two SMD peaks in mid-May and mid-July above 50 mm. However, rainfall in late May - early June decreased SMD and led to infiltration in early June. Rainfall ~~of~~during July-August also decreased SMD but did not lead to infiltration~~ED~~, which occurred~~occurred~~ring later in September. In total, 95 days of infiltration~~infiltration~~ occurred during the year 2017, mainly between January and March (42 days), September and December (46 days) but also ~~very~~ briefly in June (5 days) and August (2 days). Depth to GWL (DGWL) for both sites is shown in **Figure 4c**. At MS, DGWL was between 2 and 10 m with variations through the year. Depth to GWL increased in April (to reach 8-10 m) due to low rainfall and high SMD and

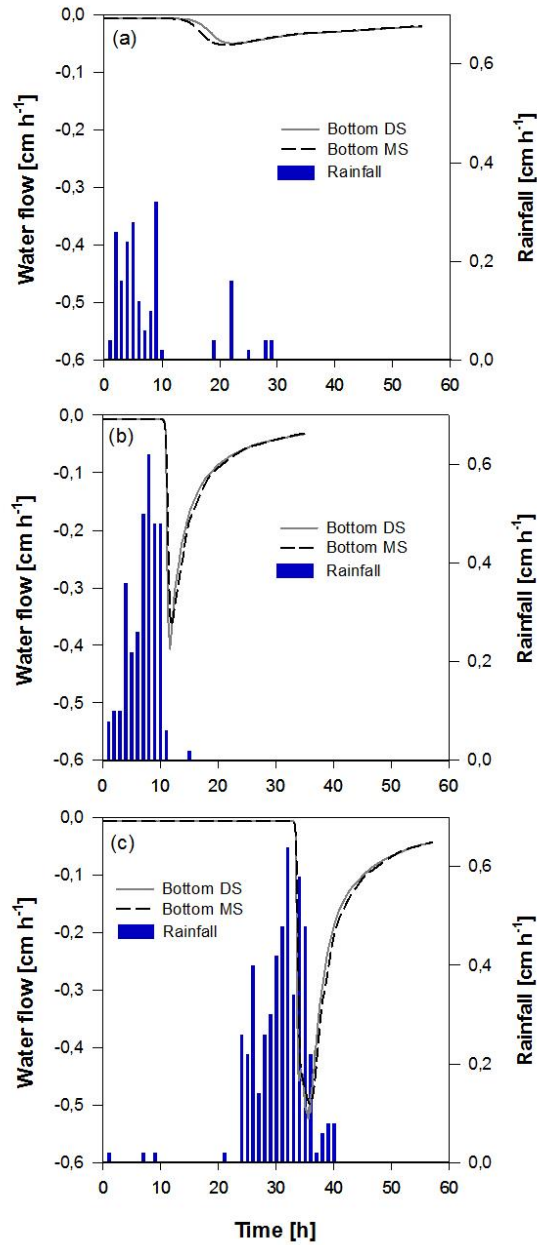


remained high until September-October. At this time of the year and until December, DGWL was lower due to low SMD and high rainfall leading to infiltration and GW recharge. At DS, DGWL was lower than at MS (up to 40 cm in April-September) with GWL sometimes above the ground level (September-December).

Over the year 2017, concentrations in TDP were higher at DS than at MS with ~~a higher variability in~~ concentrations at DS (**Fig. 4a**). In particular, TDP concentrations at DS were variable and on some occasions comparable to concentrations at MS ~~on some occasions between (January and, February, April, June)~~ whereas they remained elevated and were higher than at MS~~contrasted from on other occasions (March, May, July to -December)~~.

### 3.3. Modelled water flow~~hydrological transport to groundwater~~

Modelled water flow ~~tracer~~-breakthrough curves at the bottom of the DS and MS soil profiles are shown in **Figure 6** for each rainfall event R1 [B; long duration with low total rainfall] (**Fig. 6a**), R2 [D; short duration with high total rainfall] (**Fig. 6b**) and R3 [E; long duration with high total rainfall] (**Fig. 6c**). It should be noted that the upper boundary condition (atmospheric) was violated 63 % of the time for R3 at DS when the GWL was above ground level. The lower boundary condition (free drainage) was also violated at DS as the depth to GWL was less than 55 cm. Cumulative flow, flow first occurrence and flow peak timing and intensity are shown in Table 5. Tracer first and last occurrences, concentration peak and total transport duration ~~Modelled~~ water mass balance was equal to 0.0 % indicating the good performance of the models~~are shown in Table 3.~~



474

475 | Figure 6: Water flow ~~Tracer~~ breakthrough curves at the bottom of the soil profiles DS and MS  
 476 | for rainfall events (a) R1 [B; long duration with low total rainfall], (b) R2 [D; short duration  
 477 | with high total rainfall] and (c) R3 [E; long duration with high total rainfall].

Table 53: Water flow ~~Tracer~~-breakthrough characteristics at sites DS and MS for rainfall events R1, R2 and R3.

<u>Site</u>	<u>Rainfall event</u>	<u>Cumulative water flow</u> <u>[cm - % total rainfall]</u>	<u>Water flow first occurrence</u> <u>[h]</u>	<u>Water flow peak</u> <u>[h]</u>	<u>Water flow peak</u> <u>[cm h<sup>-1</sup>]</u>
<u>DS</u>	<u>R1</u>	<u>1.4 – 74 %</u>	<u>17</u>	<u>22.5</u>	<u>0.05</u>
	<u>R2</u>	<u>2.5 – 76 %</u>	<u>11</u>	<u>11.7</u>	<u>0.41</u>
	<u>R3</u>	<u>4.0 – 78 %</u>	<u>33</u>	<u>35.4</u>	<u>0.52</u>
<u>MS</u>	<u>R1</u>	<u>1.5 – 79 %</u>	<u>15</u>	<u>20.5</u>	<u>0.05</u>
	<u>R2</u>	<u>2.5 – 76 %</u>	<u>11</u>	<u>12.2</u>	<u>0.35</u>
	<u>R3</u>	<u>4.1 – 80 %</u>	<u>33</u>	<u>35.4</u>	<u>0.49</u>

Cumulative water flow at the bottom of the soil profiles ranged from 74 to 80 % of total rainfall input and was similar between DS and MS during R2 and higher at MS than at DS during R1 and R3. Cumulative water flow was equal to 1.4, 2.5 and 4.0 cm at DS after rainfall events R1, R2 and R3, respectively. It was equal to 1.5, 2.5 and 4.1 cm at MS after these same events. First occurrence of water flow, resulting from the rainfall event, at the bottom of the soil profiles occurred at the same time for both sites DS and MS (during R2 and R3: after 11 and 33 h, respectively) or earlier at MS than at DS (during R1: after 17 and 15 h at DS and MS, respectively). Water flow peak occurred earlier at DS (11.7 h) than at MS (12.2 h) during R2 and earlier at MS (20.5 h) than at DS (22.5 h) during R1. Its intensity was similar between DS and MS during R1 and higher at DS (0.41 – 0.52 cm h<sup>-1</sup>) than at MS (0.35 – 0.49 cm h<sup>-1</sup>) during R2 and R3.

For both sites DS and MS, cumulative water flow was the lowest during R1 [B; long duration with low total rainfall] and the highest during R3 [E; long duration with high total rainfall].

Water flow first occurrence and flow peak occurred earlier during R2 [D; short duration with high total rainfall] and later during R3 where flow peak intensity was also the highest. Water flow peak intensity was the lowest during R1.

#### 4. Discussion

This study ~~investigathighlighted~~ the spatial variability in water flow dynamics ~~the spatial variability of P in soil profiles hydrological transport through the soil profile of two locations to GW along within~~ a hillslope of contrasting GW P concentrations, and examined the inter-annual ~~variability in water flow dynamicsvariability o~~ and GW P concentrationsf GW P concentrations. A range of modelled soil hydraulic properties and subsurface water flow dynamics transport capacities were identified to 1) determine static soil properties controlling water flow at different hillslope locations and 2) determine dynamic physical controls on temporal variations in water flow and shallow GW P concentrations to suggest potential mitigation strategies to reduce P transport to GW. ~~4) determine static soil hydraulic properties controlling hydrological transport to GW along the hillslope, 2) examine variations in GW P concentrations in relation to dynamic physical controls and 3) reveal contrasting physical controls on the potential for P transport to GW at the hillslope scale.~~ The combined analysis of high resolution meteorological data, ~~high resolution~~ soil physical/hydraulic data and GW chemical data revealed ~~contrasting contrasting~~ spatial (soil) and temporal (rainfall, GWL) water flow dynamics, and subsequent P transport and attenuation potential, at different hillslope locations.

~~P hydrological transport potential to GW along the hillslope in relation to the existence of a static system (soil) and a dynamic system (rainfall, GWL, soil moisture), respectively. The DS zone showed a higher hydrological transport potential with favourable soil properties and~~

geochemical processes towards high and variable GW P concentrations. The MS zone was characterised by limited hydrological transport potential.

#### 4.1. Spatial variability in subsurface water flow ~~Spatial variability in hydrological transport~~ to groundwater

The potential for hydrological transport to GW varies within the same hillslope and ~~is determined~~ is determined by soil physical and hydraulic properties, which also influence P sorption in the USZ and P transport to GW. ~~—~~The undisturbed soil cores ~~study~~ studied suggested that ~~the DS zone had there was a lower~~ higher potential for hydrological ~~P~~ transport ~~than the MS zone to GW in the DS zone (Fig. 7)~~ due to a lower soil  $K_s$ , critical for water flow, despite its lower soil compaction (bulk density  $\rho_b$ ) and higher soil  $\phi$  and macroporosity. In contrast, the higher soil  $K_s$  in the MS zone, and despite its higher soil  $\rho_b$ , lower soil  $\phi$  and macroporosity, suggested a higher potential for vertical water flow in this zone (Fig. 7). However, water flow modelled at the bottom of the soil profiles using Hydrus 1D (Fig. 6) did not clearly reflected the differences in soil  $K_s$  between DS and MS. Higher water flow peaks at DS (Table 4, Fig. 6) during high total rainfall events indicated the higher potential for water flow though the USZ at this site, even though water flow first occurrence did not appear earlier than at MS. In contrast, lower water flow peaks at MS (Table 4, Fig. 6) during high total rainfall events indicated the lower potential for water flow though the USZ at this site. Cumulative flow at the bottom of the soil profiles, lower at DS than at MS, and independently of the rainfall event (Table 4), reflected the differences in soil  $\theta_s$  and soil water storage capacity which were higher at DS. However, as the depth to GWL was less than 55 cm at DS and was higher than 55 cm at MS, stronger differences in the timing and intensity of water flow reaching GW should be expected. High temporal resolution monitoring of GWL (Fig. 4c) also revealed a quick recharge of the aquifer at DS (although

GWL is higher at this location) after rainfall events with a slow recovery to original water table positions whereas at MS response to rainfall was slower. ~~soil  $K_s$ . This was supported by the Hydrus 1D scenario modelling, where flashier tracer transport and higher concentration peaks were evident (Table 3, Fig. 6), and which was independent of the type of rainfall event (duration, total rainfall). In contrast, the MS zone was more compacted (higher soil  $\rho_b$ ) with lower soil  $K_s$ , suggesting an attenuation of hydrological P transport to GW (Fig. 7). This was supported by the modelling indicating longer total tracer transport duration with lower concentration peaks, independent of the type of rainfall event, even though the tracer first occurrence appeared earlier in the MS zone (Table 3, Fig. 6). Higher  $\phi$ ,  $c$  and macroporosity measured from undisturbed soil cores were also characteristics of the DS zone supporting the higher potential for hydrological P transport in this zone. High temporal resolution monitoring of GWL (Fig. 4c) also revealed a quick recharge of the aquifer at DS (although GWL is higher at this location) after rainfall events with a slow recovery to original water table position whereas at MS reaction to rainfall was slower.~~

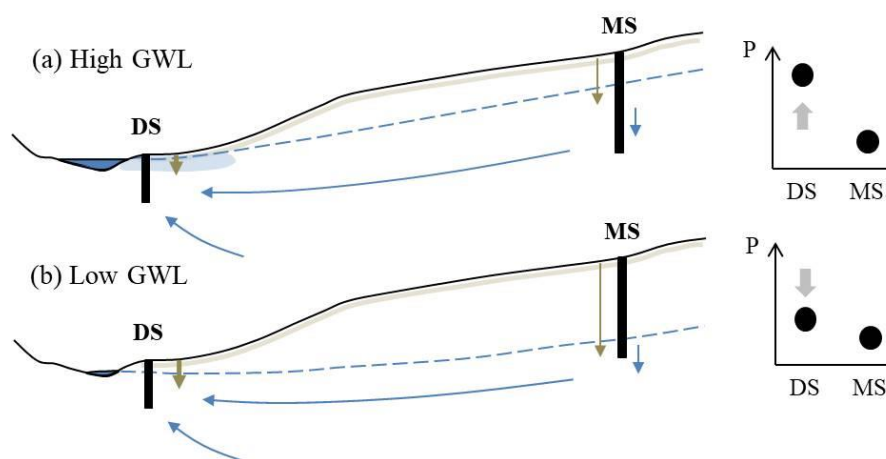


Figure 7 (in color): Schematic of contrasting groundwater P concentrations scenarios: (a)

High GWL: contrasting concentrations between the DS and MS zones with higher P

concentrations ~~at in the DS zone~~ due to the hydrological connection with soil P and (b) Low  
GWL: lower concentrations at DS and similar to concentrations between the DS and MS  
~~zones with lower P concentrations in the DS zone~~ due to the hydrological disconnection with  
soil P. In both scenarios ~~the DS zone soil properties facilitate evidence a higher potential for~~  
subsurface P water flow to shallow GW. hydrological transport to groundwater: shorter  
transport duration through the soil profile and transport distance to groundwater.

Observed ~~spatial~~ variability of soil hydraulic properties and water flow is supported to some  
extent by DeFauw et al. (2014) who observed no significant differences in infiltration  
dynamics between evaluated hydraulic properties of surface soils at varying micro-  
topographic positions and found that the infiltration rates were approximately twofold higher  
at the micro-topographic low position (thicker soil) and than at the high position (thinner  
soil). However, ~~Hendrayanto et al. (1999) observed smaller soil  $K_s$  at upper slope locations~~  
compared to mid-slope or down-slope locations, which has not been observed in this study  
and may be related to the high variability between replicates. Differences in soil texture and  
PSD, related to the slope position, may explain the differences of soil hydraulic properties  
between DS and MS, since hydraulic conductivities are coupled to the grain size distribution  
of soils (Mahmoodlu et al., 2016; Pachepsky and Rawls, 2003; Pachepsky et al., 2006).  
However, other studies found that saturated hydraulic properties at the position with a thinner  
soil were higher than at the position with a thicker soil (Dai et al., 2019).  
In this study, there was no significant difference in soil thickness at DS and MS (**Table 2**).  
However, there was a difference in soil texture. In this study, soil  $\rho_b$  and  $\phi$  were linked to soil  
PSD percentage of sand, silt and clay and indicated that sandy soils enhance water flow  
whereas have more potential for hydrological transport to GW whereas clay soils can  
attenuate– it. Moreover, and even though both sites are under grassland with large root

systems, the higher soil OM % at DS was reflected in the higher soil porosity which can be related due to greater formation and hierarchy of aggregates (Daynes et al., 2013; Hirmas et al., 2013). Annual cropping activities with heavy machinery, more frequent in the MS zone (fertilization, grass harvesting, grazing) than in the DS zone (grazing, fertilization), can also contribute to the higher soil  $\rho_b$  compaction, lower soil macroporosity (Pagliai et al., 2004) and soil OM % (Franzluebbers et al., 2014; Gimenez et al., 2002) observed at MS and influence water infiltration.

transport

However, this study focused only on the first 55 cm of soil and incorporated some uncertainties regarding the vertical variations of soil hydraulic properties at DS where two consecutive horizons were assumed to be similar to model water flow. It is also difficult to estimate water flow reaching GW in the MS zone where the GW table is deeper. Further work is needed to have a better understanding of the vertical physical heterogeneity of the deeper soil, especially where the GW table is deeper. Despite these limitations, the results indicate that there is less time for P sorption to occur in the DS zone as water flow is a quicker process. Interaction between soil solution P and the soil matrix is also likely reduced due to more water flowing via macropores and bypassing the sorption sites at DS. These hypotheses should be further investigated by incorporating soil chemical data in the models to account for P transport including colloidal P. Mitigation strategies to reduce GW P concentrations should prioritize the DS zone even though deeper GW flowpaths from the MS zone or upslope could be a potential source of P to the DS zone.

as soil  $c$  was negatively correlated to the percentage clay. Even if soil  $\rho_b$  increased with depth at both sites and may thus attenuate hydrological transport along the soil profile, the shallower GWL at DS may reach the upper soil layers exhibiting higher hydrological transport potential and lead to shorter P transport distances (Fig. 7).



However, the present study focused only on the topsoil (first 40 cm) and further work is needed to have a more complete understanding of the vertical physical variability/heterogeneity of the deeper soil, especially where the GW table is deeper as it is the case at the MS location. Soil chemical properties have also to be considered, especially in soils rich in P-binding materials (Fe, Al, Ca, clay, OM), to take into account possible attenuation processes (sorption/desorption, precipitation/dissolution) occurring along the soil profiles and controlling P transport to GW (timing, concentration). For this transect in particular, the DS zone showed evidence of higher soil OM %, labile inorganic P and degree of P saturation (DPS) (measured in composite soil samples not presented here) that could enhance the amount of P transported to GW whereas the MS zone evidence higher soil total Fe possibly attenuating P transport.

#### 4.2. Inter-annual variability in subsurface water flow ~~Inter-annual variability in hydrological transport~~ to groundwater

The potential for hydrological transport to GW, and subsequent P transport, also varied within the same hillslope zone and appeared to be linked to the inter-annual dynamic of other physical controls such as (GWL, soil moisture, rainfall and GWL), as observed over the year 2017. Modelling of water flow at the bottom of the soil profiles during contrasting rainfall events using Hydrus 1D showed that rainfall pattern influenced water flow. It was flashier with higher flow peaks during the high total rainfall events than during the low total rainfall event which suggested less time for P attenuation processes to occur when water flows during short and intense rainfall events and during longer rainfall events of autumn-winter leading to higher GW P concentrations.

Moreover, seasonal variations in GW P concentrations revealed at the DS zone by monthly monitoring appeared to be controlled by GWL fluctuations. ~~Seasonal variations in GW P concentrations revealed at the DS zone by monthly monitoring appeared to be, in part, controlled by GWL fluctuations. Shallow GW, especially after rainfall events or (August – December) during wet periods (August – December) (Fig. 4c, Fig. 7a), may lead to lower water flow travel time through the USZ, compared to dry periods where the GWL is deeper, and further reduce P attenuation processes. It may also lead to reductive dissolution of soil Fe hydroxides being solubilised as Fe<sup>2+</sup> and releasing P previously adsorbed (Vidon et al., 2010), a mechanism observed under anoxic conditions.~~ This can be important in ~~the DS~~ this zone ~~where~~ where shallow GW can connect with and mobilise a higher soil P source as chemical tests on composite soil samples revealed a higher soil labile inorganic P content (90 mg kg<sup>-1</sup>) and DPS (-8.3 %) at DS than at the MS ~~zone~~ (45 mg kg<sup>-1</sup> and 4.0 %, respectively) ((Fresne et al., 2020) not presented here), where GWL is also deeper. Previous GW monitoring ~~of the GW~~ also showed low N-NO<sub>3</sub><sup>-</sup> concentration (mean annual concentrations of 0.03 ± 0.01 mg L<sup>-1</sup>) due to denitrifying conditions (mean annual ORP of 6.0 ± 1.8 mV) (McAleer et al., 2017) and higher Fe (4-712 ± 1-526 µg L<sup>-1</sup>) and Mn (2-928 ± 197 mg L<sup>-1</sup>) concentrations at DS than compared to at the MS zone; this supports the hypothesis of Fe oxyhydroxide reduction. Organic riparian soils are known as internal sources of soluble reactive P (Dupas et al., 2017b; Gu et al., 2017; Records et al., 2016) due to poor retention capacities (Daly et al., 2001; Roberts et al., 2017) and where soil solution P concentrations have been strongly linked to GWL dynamics (Dupas et al., ~~(2015)~~ In contrast, showed that soil solution P concentrations in riparian wetlands were strongly linked to GWL dynamics. Shallow GWL may connect with and mobilise more soil P as the pool and/or mobility of soil P decreases with depth, this is especially important as a higher soil labile

inorganic P content has been measured at DS compared to MS. Organic riparian soils are known as internal sources of soluble reactive P (Dupas et al., 2017b; Gu et al., 2017; Records et al., 2016) due to poor retention capacities (Daly et al., 2001; Roberts et al., 2017) and their high proportion in a catchment has been strongly related to higher stream soluble reactive P concentrations (Dupas et al., 2018). At the MS zone, the soil showed lower soil labile inorganic P, DPS and higher total Fe contents than at DS possibly attenuating P in GW, also deeper at this location. Moreover, hydrochemical GW data ~~at MS~~ revealed nitrification processes (mean annual ORP of  $162.5 \pm 3.5$  mV) occurring (McAleer et al., 2017). This site had higher annual mean  $\text{N-NO}_3^-$  concentration ( $7.21 \pm 0.38$  mg L<sup>-1</sup>) but lower Fe ( $3.85 \pm 0.87$  µg L<sup>-1</sup>) and Mn concentrations ( $2.87 \pm 0.74$  mg L<sup>-1</sup>) than at ~~the DS zone~~. This suggests that reduction of Fe hydroxides is limited and may support lower GW P concentrations measured at this site. However, as the GW table sinks during dry periods in the DS zone in April, or later in the year in the MS zone (**Fig. 7b**), it may leave the higher P sources in the topsoil disconnected and increase water flow travel time enhancing P attenuation processes.

However, P concentrations measured in GW can result from a combination of vertical P leaching from soil and lateral flows within the aquifer transporting P from the upper hillslope which are not considered here. Further work is needed including acquisition of higher resolution GW chemical data to get a better understanding of the main processes explaining inter-annual P dynamics, especially in the near stream zone DS. Inclusion of the different P species and fractions, including colloidal P (1-1000 nm), would be an important improvement into understanding such processes. Remediation measures should prioritise reducing the source of soil P source at DS by limiting the timing and/or the intensity of the grazing period especially during periods of higher GWL table that may mobilise P. Reduction of P

applications (as synthetic or organic fertilizers) on the MS zone and the upslope should also be considered. -

Soil moisture conditions also appeared to be important as soil rewetting after dry periods could explain peaks in GW P concentrations in May (**Fig. 4a, 4b**), revealed by monthly GW monitoring, through release of microbial P by osmotic shock (Blackwell et al., 2010; Turner and Haygarth, 2001) or loss of colloidal P (1-1000 nm) via preferential flowpaths in macropores (Poulsen et al., 2006; Vendelboe et al., 2011). Moreover, monthly monitoring of GW also revealed contrasting P concentrations between February (DS lower and comparable to MS) and October (DS higher, MS lower) where soil moisture conditions were comparable (**Fig. 4a, 4b**). This could be related to rainfall patterns as the Hydrus 1D scenario modelling showed that tracer first occurrence and peak appeared earlier during rainfall event R3 [October; long duration with high total rainfall] than during rainfall event R1 [February; long duration with low total rainfall]. Tracer total transport duration was also lower during rainfall event R3 than R1 (**Table 3**) suggesting that P reaction time with the soil matrix is lower and attenuation processes are more limited during this type of rainfall event, thus potentially explaining higher GW P concentrations.

However, P concentrations measured in GW can result from a combination of vertical P leaching from soil and lateral flows within the aquifer transporting P from the upper hillslope which are not considered here. Further work is needed including acquisition of higher resolution GW chemical data to get a better understanding of the main processes explaining inter-annual P dynamics, especially in the near stream zone DS. Inclusion of the different P species and fractions, including colloidal P, would be an important improvement into understanding such processes. Monitoring of stream P fractions and species and

determination of hydrological pathways would also be important to determine the contribution of the different hillslope zones. Indeed, previous research in catchments with similar shallow GW systems and presence of riparian wetlands have shown that seasonal variability of stream soluble reactive P was linked to the contribution of different hillslope compartments (Dupas et al., 2017a).

## 5. Conclusion

Both static and dynamic factors influence water flow through the USZ hillslope P transport to shallow GW, controlling soil P attenuation processes, and therefore can therefore contribute to spatial and temporal variations in GW P concentrations ~~can vary both spatially and temporally over short distances~~. Herein~~In this study~~, two conceptual views of the hillslope emerged. The first corresponds to variable concentration at DS, on some occasions low and similar and low to concentrations ~~between the DS and at MS zones~~ due to less connection between GW and soil P (lower GWL), and slower water flow and also longer water P travel time to GW ~~within the soil profile where P attenuation processes can occur~~, even though the DS zone has more potential for hydrological transport than the MS zone due to its soil physical physical and hydraulic properties. — The second corresponds to contrasting concentrations between ~~the DS and MS zones~~ with ~~the DS zone~~ becoming temporally elevated due to the hydrological connection (~~high GWL~~) with soil P (higher GWL), flashier water flow and ~~and~~ shorter water travel time to GW ~~within the soil profile~~. Hence, — soil physical and hydraulic properties control are important for water flow and travel time hydrological transport to GW, and subsequent P transport to GW, and should be considered to better target cost-effective mitigation measures. R by prioritising ~~reduction of P sources (from grazing or fertilization~~ limitation, reduction of P applications on the connected hillslope) should be prioritized in zones of higher potential for hydrological transport or

~~shallow GWL as the near-streamthe DS zones. Here they are characterised by a lower soil compaction, higher  $K_s$ , and a sandy soil texture.~~

## Author contribution

MF: Conceptualization, Methodology, Validation, Formal analysis, Investigation, Data curation, Writing – original draft, Writing – reviewing and editing, Visualization. OF: Conceptualization, Methodology, Validation, Resources, Writing – reviewing and editing, Supervision. PEM: Conceptualization, Methodology, Resources, Writing – reviewing and editing, Funding acquisition. PJ and KD: Conceptualization, Methodology, Writing – reviewing and editing.

## Competing interests

The authors declare that they have no conflict of interest.

## Acknowledgements

We thank the ACP land owners and farmers of the fields for cooperation and sampling permission, the ACP staff especially David Ryan and Dermot Leahy for field sampling assistance, Una Cullen for meteorological and GW level data supply. The lab work of Shane Scannell for bulk density analyses is greatly appreciated. We also thank Matthias Bacher for Hyprop training and Cathal Somers for help in Hyprop lab set up and particle size analyses. Funding was provided by the Department of Agriculture, Food and the Marine through the Teagasc Agricultural Catchments Programme and by the Teagasc Walsh Fellowship Programme.

## References

763 Agah, A. E., Meire, P., and Deckere, E.: Simulation of phosphorus transport in soil under  
 764 municipal wastewater application using hydrus-1D. In: Soil contaminations - Current  
 765 consequences and further solutions, InTech, 177-190, 2016.

766 Anderson, A. E., Weiler, M., Alila, Y., and Hudson, R. O.: Dye staining and excavation  
 767 of a lateral preferential flow network, Hydrol. Earth Syst. Sci., 13, 935–944, 2009.

768 Askew, F. E.: Persulfate method for simultaneous determination of total nitrogen and total  
 769 phosphorus. 4500-P J, in: Eaton, A. D., Clesceri, L. S., Rice, W. E., and Greenberg, A. E.,  
 770 editors. Standard Methods for the Examination of Water and Wastewater, 21<sup>st</sup> edition. ISBN  
 771 0-87553-047-8. 800 1 street, NW Washington, DC 2001-3710: American Public Health  
 772 Association, 160-161, 2005.

773 Askew, F. E. and Smith, R. K.: Inorganic non metallic constituents; Phosphorus; Method  
 774 4500-P F. Automated ascorbic acid reduction method, in: Eaton, D. A., Clesceri, L. S., Rice,  
 775 E. W., and Greensberg, A. E., editors. Standard Methods for the Examination of Waters and  
 776 Waste Water. 800 1 street, NW Washington, DC 2001-3710: ISBN 0-87553-047-8 American  
 777 Public Health Association, 4-155, 2005.

778 Avery, B. W. and Bascomb, C. L.: Soil survey laboratory methods.: Soil Survey of Great  
 779 Britain (England and Wales), Harpenden (Rothamsted Experimental Station, Harpenden,  
 780 Herts.), 1974.

781 Bacher, M. G., Schmidt, O., Bondi, G., Creamer, R., and Fenton, O.: Comparison of Soil  
 782 Physical Quality Indicators Using Direct and Indirect Data Inputs Derived from a  
 783 Combination of In-Situ and Ex-Situ Methods, Soil Science Society of America Journal, 83,  
 784 5-17, 2019.

785 Bachmair, S. and Weiler, M.: Hillslope characteristics as controls of subsurface flow  
 786 variability, Hydrol. Earth Syst. Sci., 16, 3699–3715, 2012a.

787 Bachmair, S., Weiler, M., and Troch, P. A.: Intercomparing hillslope hydrological  
788 dynamics: spatio-temporal variability and vegetation cover effects, *Water Resour. Res.*, 48,  
789 2012b.

790 Bezerra-Coelho, C. R., Zhuang, L., Barbosa, M. C., Soto, M., and van Genuchten, M. T.:  
791 Further tests of the HYPROP evaporation method for estimating the unsaturated soil  
792 hydraulic properties, *Journal of Hydrology and Hydromechanics*, 66(2), 161-169, 2018.

793 Bol, R., Julich, D., Bröddlin, D., Siemens, J., Kaiser, K., Dippold, M. A. et al.: Dissolved  
794 and colloidal phosphorus fluxes in forest ecosystems—an almost blind spot in ecosystem  
795 research, *J Plant Nutr Soil Sci.*, 179, 425-438, 2016.

796 Brady, N.C. and Weil, R. R.: *The Nature and Properties of Soils*, 14<sup>th</sup> Edition. United  
797 States of America: Pearson Education Inc., 2008.

798 Bünemann, E. K., Bongiorno, G., Bai, Z., Creamer, R. E., De Deyn, G., de Goede, R. et  
799 al.: Soil quality – A critical review, *Soil Biology and Biochemistry*, 120, 105-125, 2018.

800 Cordell, D. and White, S.: Life's Bottleneck: Sustaining the World's Phosphorus for a  
801 Food Secure Future, *Annual Review of Environment and Resources*, 39, 161, 2014.

802 Daly, K., Jeffrey, D., and Tunney, H.: The effect of soil type on phosphorus sorption  
803 capacity and desorption dynamics in Irish grassland soils, *Soil Use Manage.*, 17, 12-20, 2001.

804 Daynes, C. N., Field, D. J., Saleeba, J. A., Cole, M. A., and McGee, P. A.: Development  
805 and stabilisation of soil structure via interactions between organic matter, arbuscular  
806 mycorrhizal fungi and plant roots, *Soil biology & biochemistry*, 57, 683-694, 2013.

807 DeFauw, S. L., Brye, K. R., Sauer, T. J., and Hays, P.: Hydraulic and Physiochemical  
808 Properties of a Hillslope Soil Assemblage in the Ozark Highlands, *Soil Sci.*, 179(3), 107-117,  
809 2014.



810 Duan, J., Yang, J., Tang, C., Chen, L., Liu, Y., and Wang, L.: Effects of rainfall patterns  
811 and land cover on the subsurface flow generation of sloping Ferralsols in southern China,  
812 PLOS ONE, 12(8), 2017.

813 Dupas, R., Gruau, G., Gu, S., Humbert, G., Jaffrézic, A., and Gascuel-Oudou, C.:  
814 Groundwater control of biogeochemical processes causing phosphorus release from riparian  
815 wetlands, Water Research, 84, 307-314, 2015.

816 Dupas, R., Mellander, P-E., Gascuel-Oudou, C., Fovet, O., McAleer, E. B., McDonald, N.  
817 T. et al.: The role of mobilisation and delivery processes on contrasting dissolved nitrogen  
818 and phosphorus exports in groundwater fed catchments, Science of The Total Environment,  
819 599-600, 1275-1287, 2017a.

820 Dupas, R., Musolff, A., Jawitz, J. W., Rao, P. S. C., Jäger, C. G., Fleckenstein, J. H. et al.:  
821 Carbon and nutrient export regimes from headwater catchments to downstream reaches,  
822 Biogeosciences, 14, 4391–4407, 2017b.

823 Durner, W.: Hydraulic conductivity estimation for soils with heterogeneous pore  
824 structure, Water Resour Res., 30, 211-223, 1994.

825 Elmi, A., Abou Nohra, J. S., Madramootoo C. A., and Hendershot, W.: Estimating  
826 phosphorus leachability in reconstructed soil columns using HYDRUS-1D model, Environ  
827 Earth Sci, 65, 1751-1758, 2012.

828 Fealy, R. M., Buckley, C., Mehan, S., Melland, A., Mellander, P-E., Shortle, G. et al.:  
829 The Irish Agricultural Catchments Programme: catchment selection using spatial multi-  
830 criteria decision analysis, Soil Use Manage., 26, 225-236, 2010.

831 Fenton, O., Vero, S., Ibrahim, T. G., Murphy, P. N. C., Sherriff, S. C., and Ó hUallacháin,  
832 D.: Consequences of using different soil texture determination methodologies for soil  
833 physical quality and unsaturated zone time lag estimates, Journal of Contaminant Hydrology,  
834 182, 16-24, 2015.

835 Fenton, O., Mellander, P-E., Daly, K., Wall, D. P., Jahangir, M. M. R., Jordan, P. et al.:  
836 Integrated assessment of agricultural nutrient pressures and legacies in karst landscapes,  
837 Agriculture, Ecosystems & Environment, 239, 246-256, 2017.

838 Franzluebbers, A. J., Sawchik, J., and Taboada, M. A.: Agronomic and environmental  
839 impacts of pasture–crop rotations in temperate North and South America, Agriculture,  
840 ecosystems & environment, 190, 18-26, 2014.

841 Fresne, M., Jordan, P., Fenton, O., Mellander, P-E., and Daly, K.: Soil chemical and  
842 fertilizer influences on soluble and medium-sized colloidal phosphorus in agricultural soils,  
843 Science of the total environment, 142112, 2020.

844 Fuchs, J. W., Fox, G. A., Storm, D. E., Penn, C. J., and Brown, G. O.: Subsurface  
845 Transport of Phosphorus in Riparian Floodplains: Influence of Preferential Flow Paths,  
846 Journal of Environmental Quality, 38(2), 473-484, 2009.

847 Gao, Y., Zhu, B., Wang, T., Tang, J. L., Zhou, P., and Miao, C. Y.: Bioavailable  
848 phosphorus transport from a hillslope cropland of purple soil under natural and simulated  
849 rainfall, Environmental Monitoring and Assessment, 171, 539-550, 2010.

850 Giménez, D., Karmon, J. L., Posadas, A., and Shaw, R. K.: Fractal dimensions of mass  
851 estimated from intact and eroded soil aggregates, Soil & tillage research, 64, 165-172, 2002.

852 Gladnyeva, R. and Saifadeen, A. Effects of hysteresis and temporal variability in  
853 meteorological input data in modelling of solute transport in unsaturated soil using Hydrus-  
854 1D, Journal Of Water Resources Planning And Management, 68, 285-293, 2013.

855 Gottler, R. A., and Piwoni, M. D.: Metals.  
856 Method 3120 B. Inductively coupled plasma (ICP) method, in: Eaton, D. A., Clesceri, L. S.,  
857 Rice, E. W., and Greensberg, A. E., editors. Standard Methods for the Examination of Waters  
858 and Waste Water. 21st ed. 800 1 street, NW Washington, DC 2001-3710: American Public  
859 Health Association, 3-39, 2005.

Graham, C. B., Woods, R. A., and McDonnell, J. J.: Hillslope threshold response to rainfall: (1) A field based forensic approach, *J. Hydrol.*, 393, 65–76, 2010.

Gu, S., Gruau, G., Dupas, R., Rumpel, C., Crème, A., Fovet, O. et al.: Release of dissolved phosphorus from riparian wetlands: Evidence for complex interactions among hydroclimate variability, topography and soil properties, *Science of The Total Environment*, 598, 421-431, 2017.

Guo, L., Lin, H., Fan, B., Nyquist, J., Toran, L., and Mount, G. J.: Preferential flow through shallow fractured bedrock and a 3D fill-and-spill model of hillslope subsurface hydrology, *Journal of Hydrology*, 576, 430-442, 2019.

Hendrayanto, Kosugi, K., Uchida, T., Matsuda, S., and Mizuyama, T.: Spatial Variability of Soil Hydraulic Properties in a Forested Hillslope, *J For Res*, 4, 107-114, 1999.

Hirmas, D. R., Giménez, D., Subroy, V., Platt, B. F.: Fractal distribution of mass from the millimeter- to decimeter-scale in two soils under native and restored tallgrass prairie, *Geoderma*, 207-208, 121-130, 2013.

Ibrahim, T. G., Fenton, O., Richards, K. G., Fealy, R. M., and Healy, M. G.: Spatial and temporal variations of nutrient loads in overland flow and subsurface drainage from a marginal land site in south-east Ireland, *Biology and Environment: Proceedings of the Royal Irish Academy*, 113B(2), 1-18, 2013.

Jacques, D., Šimůnek, J., Mallants, D., and van Genuchten, M. T.: Modelling coupled water flow, solute transport and geochemical reactions affecting heavy metal migration in a podzol soil, *Geoderma*, 145, 449-461, 2008.

Julich, D., Julich, S., and Feger, K.: Phosphorus fractions in preferential flow pathways and soil matrix in hillslope soils in the Thuringian Forest (Central Germany), *J Plant Nutr Soil Sci.*, 180, 407-417, 2017.

884 Kamphake, L. J., Hannah, S. A., and Cohen, J. M.: Automated analysis for nitrate by  
885 hydrazine reduction, *Water Res.*, 1, 205-216, 1967.

886 Kurz, I., Coxon, C., Tunney, H., and Ryan, D.: Effects of grassland management practices  
887 and environmental conditions on nutrient concentrations in overland flow, *Journal of*  
888 *Hydrology*, 304, 35-50, 2005.

889 Lehmann, P., Hinz, C., McGrath, G., Tromp-van-Meerveld, H. J., and McDonnell, J. J.:  
890 Rainfall threshold for hillslope outflow: an emergent property of flow pathway connectivity,  
891 *Hydrol. Earth Syst. Sci.*, 11, 1047-1063, 2007.

892 Lintern, A., Webb, J. A., Ryu, D., Liu, S., Bende-Michl, U., Waters, D. et al.: Key factors  
893 influencing differences in stream water quality across space. *WIREs Water*, 5: e1260, 2018.

894 Mabilde, L., De Neve, S., and Sleutel, S.: Regional analysis of groundwater phosphate  
895 concentrations under acidic sandy soils: Edaphic factors and water table strongly mediate the  
896 soil P-groundwater P relation, *Journal of Environmental Management*, 203(1), 429-438,  
897 2017.

898 Mahmoodlu, M. G., Raoof, A., Sweijen, T., and van Genuchten, M. T.: Effects of Sand  
899 Compaction and Mixing on Pore Structure and the Unsaturated Soil Hydraulic Properties,  
900 *Vadose Zone Journal*, 15(8), 2016.

901 McAleer, E. B., Coxon, C. E., Richards, K. G., Jahangir, M. M. R., Grant, J., and  
902 Mellander, P-E.: Groundwater nitrate reduction versus dissolved gas production: A tale of  
903 two catchments, *Science of The Total Environment*, 586, 372-389, 2017.

904 McGinley, P. M., Masarik, K. C., Gotkowitz, M. B., and Mechenich, D. J.: Impact of  
905 anthropogenic geochemical change and aquifer geology on groundwater phosphorus  
906 concentrations, *Applied Geochemistry*, 72, 1-9, 2016.

907 Melland, A. R., Mellander, P-E., Murphy, P. N. C., Wall, D. P., Mechan, S., Shine, O. et  
 908 al.: Stream water quality in intensive cereal cropping catchments with regulated nutrient  
 909 management, *Environmental Science & Policy*, 24, 58-70, 2012.

910 Mellander, P-E., Melland, A. R., Murphy, P. N. C., Wall, D. P., Shortle, G., and Jordan,  
 911 P.: Coupling of surface water and groundwater nitrate-N dynamics in two permeable  
 912 agricultural catchments, *The Journal of Agricultural Science*, 152, 107-124, 2014.

913 Mellander, P-E., Jordan, P., Shore, M., McDonald, N. T., Wall, D. P., Shortle, G. et al.:  
 914 Identifying contrasting influences and surface water signals for specific groundwater  
 915 phosphorus vulnerability, *Science of The Total Environment*, 541, 292-302, 2016.

916 Mellander, P-E., Jordan, P., Bechmann, M., Fovet, O., Shore, M., McDonald, N. T. et al.  
 917 Integrated climate-chemical indicators of diffuse pollution from land to water, *Scientific*  
 918 *Reports*, 8, 944, 2018.

919 Mualem, Y.: A new model for predicting the hydraulic conductivity of unsaturated porous  
 920 media, *Water Resour Res.*, 12, 513-522, 1976.

921 Neidhard, H., Schoeckle, D., Schleinitz, A., Eiche, E., Berner, Z., Tram, P. T. K. et al.:  
 922 Biogeochemical phosphorus cycling in groundwater ecosystems – Insights from South and  
 923 Southeast Asian floodplain and delta aquifers, *Science of the Total Environment*, 644, 1357-  
 924 1370, 2018.

925 Pachepsky, Y. A. and Rawls, W. J.: Soil structure and pedotransfer functions, *Eur J Soil*  
 926 *Sci.*, 54, 443-452, 2003.

927 Pachepsky, Y. A., Rawls, W. J., and Lin, H. S.: Hydropedology and pedotransfer  
 928 functions, *Geoderma*, 131, 308-316, 2006.

929 Pagliai, M., Vignozzi, N., and Pellegrini, S.: Soil structure and the effect of management  
 930 practices, *Soil & tillage research*, 79, 131-143, 2004.

931 Pang, L., Lafogler, M., Knorr, B., McGill, E., Saunders, D., Baumann, T. et al.: Influence  
 932 of colloids on the attenuation and transport of phosphorus in alluvial gravel aquifer and  
 933 vadose zone media, *Science of The Total Environment*, 550, 60-68, 2016.

934 Pferdmenges, J., Breuer, L., Julich, S., and Kraft, P.: Review of soil phosphorus routines  
 935 in ecosystem models, *Environmental modelling & software : with environment data news*,  
 936 126, 104639, 2020.

937 Radcliffe, D. E., Reid, D. K., Blombäck, K., Bolster, C. H., Collick, A. S., Easton, Z. M.  
 938 et al.: Applicability of Models to Predict Phosphorus Losses in Drained Fields: A Review,  
 939 *Journal of environmental quality*, 44, 614-628, 528.

940 Records, R. M., Wohl, E., and Arabi M.: Phosphorus in the river corridor, *Earth-Science*  
 941 *Reviews*, 158, 65-88, 2016.

942 Roberts, W. M., Gonzalez-Jimenez, J. L., Doody, D. G., Jordan, P., and Daly, K.:  
 943 Assessing the risk of phosphorus transfer to high ecological status rivers: Integration of  
 944 nutrient management with soil geochemical and hydrological conditions, *Science of The*  
 945 *Total Environment*, 589, 25-35, 2017.

946 Schilling, K. E., Kim, S., Jones, C. S., and Wolter, C. F.: Orthophosphorus Contributions  
 947 to Total Phosphorus Concentrations and Loads in Iowa Agricultural Watersheds, *Journal of*  
 948 *Environmental Quality*, 46(4), 828-835, 2017.

949 Schoumans, O. F. and Groenendijk, P.: Modeling Soil Phosphorus Levels and Phosphorus  
 950 Leaching From Agricultural Land In the Netherlands, *Journal of environmental quality*,  
 951 29(1), 111-116, 2000.

952 Schoumans, O. F., Silgram, M., Groenendijk, P., Bouraoui, F., Andersen, H. E.,  
 953 Kronvang, B. et al. Description of nine nutrient loss models: capabilities and suitability based  
 954 on their characteristics, *Journal of Environmental Monitoring*, 11(3), 5066-5114, 2009.

955 Schulte, R. P. O., Diamond, J., Finkle, K., Holden, N. M., and Brereton, A. J.: Predicting  
 956 the soil moisture conditions of Irish grassland, Irish Journal of Agriculture and Food  
 957 Research, 44(1), 95-110, 2005.

958 Sharpley, A. N.: Managing agricultural phosphorus to minimize water quality impacts,  
 959 Scientia Agricola, 73(1), 1-8, 2016.

960 Šimůnek, J., van Genuchten, M. T., and Sejna, M.: Modeling subsurface water flow and  
 961 solute transport with HYDRUS and related numerical software packages. In: Navarro PG,  
 962 Playán E, editors. Numerical Modelling of Hydrodynamics for Water Resources., 2008.

963 Šimůnek, J., Šejna, M., Saito, H., Sakai, M., and van Genuchten, M. T.: The HYDRUS 1D  
 964 software package for simulating the movement of water, heat and  
 965 multiple solutes in variably saturated media. Version 4.16 HYDRUS software series  
 966 Riverside, California, USA.: Department of Environmental Science, University of California  
 967 Riverside, 2013.

968 Sinha, E., Michalak, A. M., and Balaji, V.: Eutrophication will increase during the 21st  
 969 century as a result of precipitation changes, Science, 357, 407-408, 2017.

970 Tromp-van Meerveld, H. J. and Weiler, M.: Hillslope dynamics modeled with increasing  
 971 complexity, J. Hydrol., 361, 24–40, 2008.

972 van Genuchten, M. T.: A Closed-form Equation for Predicting the Hydraulic Conductivity  
 973 of Unsaturated Soils, Soil Science Society of America journal, 44, 892-898, 1980.

974 Vereecken, H., Javaux, M., Weynants, M., Pachepsky, Y., Schaap, M., and van  
 975 Genuchten, M. T.: Using pedotransfer functions to estimate the van genuchten- mualem soil  
 976 hydraulic properties: A review, Vadose Zone Journal, 9(4), 795-820, 2010.

977 Vero, S. E., Ibrahim, T. G., Creamer, R. E., Grant, J., Healy, M. G., Henry, T. et al.:  
 978 Consequences of varied soil hydraulic and meteorological complexity on unsaturated zone  
 979 time lag estimates, Journal of Contaminant Hydrology, 170, 53-67, 2014.

980 Vidon, P., Allan, C., Burns, D., Duval, T. P., Gurwick, N., Inamdar, S. et al.: Hot Spots  
 981 and Hot Moments in Riparian Zones: Potential for Improved Water Quality Management,  
 982 Journal of the American Water Resources Association, 46, 278-298, 2010.

983 Wilson, G. V., Jardine, P. M., Luxmoore, R. J., and Jones, J. R.: Hydrology of a forested  
 984 hillslope during storm events., Geoderma ,46, 119-138, 1990.

985 Wilson, G. V., Nieber, J. L., Fox, G. A., Dabney, S. M., Ursic, M., and Rigby, J. R.:  
 986 Hydrologic connectivity and threshold behavior of hillslopes with fragipans and soil pipe  
 987 networks, Hydrol Process, 31, 2477-2496, 2017.

988 Withers, P. J. A., Neal, C., Jarvie, H. P., and Doody, D. G.: Agriculture and  
 989 Eutrophication: Where Do We Go from Here?, Sustainability, 6, 5853-5875, 2014.